Collisional regime during the discharge of a two-dimensional silo

Roberto Arévalo*

Simulation of Industrial Assets and Processes, Research Centre for Energy Resources and Consumption (CIRCE), Avenue Ranillas 3D, 1st floor, 50018 Zaragoza, Spain

(Received 15 September 2021; accepted 15 February 2022; published 6 April 2022)

The present work reports an investigation into the collisional dynamics of particles in the vicinity of the outlet of a two-dimensional silo using molecular dynamics simulations. Most studies on this granular system focus in the bulk of the medium. In this region, contacts are permanent or long-lived, so continuous approximations are able to yield results for velocity distributions or mass flow. Close to the exit, however, the density of the medium decreases and contacts are instantaneous. Thus, the collisional nature of the dynamics becomes significant, warranting a dedicated investigation as carried out in this work. More interesting, the vicinity of the outlet is the region where the arches that block the flow for small apertures are formed. It is found that the transition from the clogging regime (at small apertures) to the continuous flow regime is smooth in collisional variables. Furthermore, the dynamics of particles as reflected by the distributions of the velocities is as well unaffected. This result implies that there is no critical outlet size that separates both regimes, as had been proposed in the literature. Instead, the results achieved support the alternative picture in which a clog is possible for any outlet size.

DOI: 10.1103/PhysRevE.105.044901

I. INTRODUCTION

The discharge of a silo by gravity has been during years a favorite process to explore the dynamics of granular materials [1–15]. These media consist of macroscopic particles interacting by frictional contact forces, giving rise to a plethora of novel behaviors studied by engineers and physicists alike [16–26]. In a flat-bottomed silo (see Fig. 1), a column of particles or grains is allowed to come to rest before opening a hole at the base. Then, a stream of particles flows out of the silo, pulled by the force of gravity. Depending on the relation between the size of the particles d and that of the exit D, two main regimes can be identified. When particles are several times smaller than the exit, the flow is smooth and continuous. Like the one in an hourglass, it proceeds unperturbed and is reminiscent of the outflow of a liquid. However, due to the Janssen effect [27], the pressure is constant for most of the depth of the silo, and the flow is independent of the height of material inside the silo [28].

Upon reducing the size of the outlet ($D \lesssim 5d$), the dynamics of the flow starts to change. In Ref. [29], a sharp transition in the characteristic frequency of flow fluctuations is found and related to the stability of transitory arches even well inside the continuous regime. When the size of the particles becomes comparable to that of the exit, the flow starts to exhibit disturbances. In two dimensions, this happens when the ratio D/d of hole to grain size is around 5. Oscillations appear which grow upon further reducing the outlet size. Eventually, the flow is arrested by the formation of an arch of particles. Around $D/d = 5$, many arches are short-lived, being soon dragged by the stream of incoming particles. This results in an intermittent flow regime. Below that value, stable arches appear that are necessary to remove to resume the flow.

In the bulk of the silo, particles present a relatively high packing density and most contacts are permanent, rather than exhibiting a collisional regime. Under these conditions, the flow can be modeled as a continuous medium [30,31] to predict the shape of the velocity profile with excellent accuracy. Approaching the outlet, however, the situation changes. The packing fraction of the particles decreases quickly, and the discontinuous nature of the medium becomes more important. The low density precludes the existence of durable contacts, so the dynamics of particles is now dominated by collisions. Although a continuous description in which the relevant length scale is D is possible [32], high-speed images show the particles colliding in a way that reminds one of a gas until rather suddenly an arch is formed [33].

These two flow regimes, continuous at large values of D/d and clogging at low values, are reflected in the behavior of the mass flow of particles. In the continuous regime, the mass flow is proportional to $D^{5/2}$ in $3D$ or $D^{3/2}$ in $2D$. This scaling can be simply rationalized as the product of the area of the outlet times the typical velocity of the particles when they reach it. However, in the clogging regime the scaling of the flow grows more quickly. This is due to the variation of the packing fraction, which grows for small values of D/d until it reaches a constant value. From the point where the packing fraction saturates, the expected power law behavior of the flow is observed [34].

*rarevalo@fcirce.es

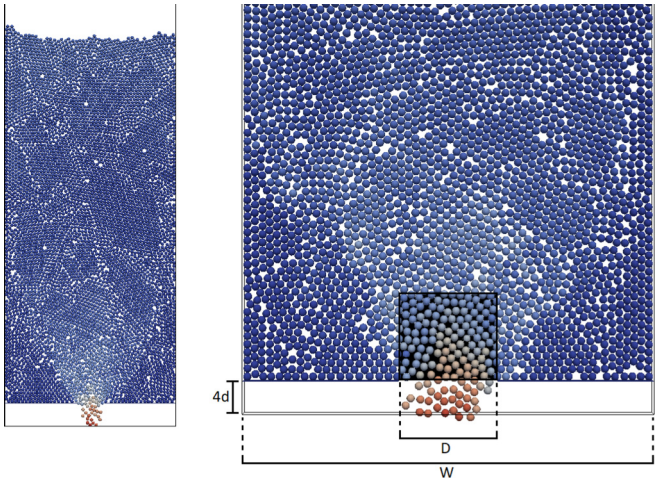

FIG. 1. Snapshot of a simulation. Left: A silo with a large aperture size flowing in steady state. Right: Region close to the exit. The shadowed square represents the $D \times D$ observation window.

A point that has been debated is whether a critical D/d ratio exists that separates the clogging regime, in which the flow is arrested by arches, from the continuous regime [35–38]. The argument in favor is that the number of grains poured out from the silo between two clogs (termed an avalanche) seems to grow as a critical power law of D/d. However, these measurements are difficult to carry out due to the fast growth of the avalanches of grains. As a consequence, the data can be fitted equally well to functions of D which present a critical value and to functions that do not. By other side, the critical exponent and the value of the critical outlet size in $2D$ ($D_c \approx 8.5d$ [36]) turn out to be rather large to be easily interpretable. The recent work [38] introduces the concept of clogging configurations to build a strong statistical argument. The conclusion is that the probability of forming an arch expanding the outlet size simply decreases until it is unobservable within experimental time windows.

The aim of the present work is to study the gaslike behavior of particles in the vicinity of the outlet during the transition from the clogging to the continuous flow regime. Unlike the approaches mentioned, ours takes at face value the collisional nature of the dynamics close to the outlet. It is found that the transition is smooth in D/d, indicating that there is no critical outlet size separating both regimes. This conclusion is reinforced by studying the collisional dynamics of the particles in the vicinity of the outlet.

II. MATERIALS AND METHODS

A. Numerical method

The present study carries out molecular dynamics simulations of granular materials using the free and open source software LIGGGHTS [39] which is an extension for granular matter of the the well-known LAMMPS [40] package. The advantage of this choice (apart of being open and free) is that LIGGGHTS has many interaction potentials already built in, including the most common for granular matter. Besides, it is efficiently implemented and parallelized for fast simulations.

The particles are modelled as monosized spheres of diameter $d = 1$ mm. In this way, we avoid introducing size segregation in the silo, which would complicate the analysis and obscure the phenomena under study. The width W of the silo is $50d$ to avoid the influence of the position of the walls [41]. The height is $100d$ for small to medium outlet size, $200d$ for the larger outlets and $220d$ for the case $D = 15d$. This height ensures that the dynamics is independent of the filling. Finally, a depth of $1.1d$ was used as is the case of some experiments [42]. The number of particles used ranges from 5000 to 10 000.

In the present work, we consider only contact forces; under this condition, two particles interact whenever their distance r_{ij} becomes smaller than the sum of their radii. To model the interaction between particles, we choose the Hertz contact, which includes both frictional and dissipative terms:

$$\mathbf{F}_n = k_n \xi \mathbf{n}_{ij} - \gamma_n v_{i,j} \mathbf{n}_{ij}, \tag{1}$$

$$\mathbf{F}_t = k_t \xi \mathbf{t}_{ij} - \gamma_t v_{i,j} \mathbf{t}_{ij}. \tag{2}$$

The first equation is the component of the force in the normal direction of the impact. The spring force is proportional to the overlap $\xi = \frac{1}{2}(d_i + d_j) - r_{ij}$ of the particles. The second term is a damping proportional to the relative velocity of the colliding particles. The parameter k_n is the elastic constant and γ_n is a viscoelastic damping constant whose role is to dissipate energy during the collision. Analogously, the force in the tangential direction depends on a restoring term, proportional to the sliding of the particles, and a damping term that dissipates energy. The damping constants are related to the restitution coefficient (see definition below). They control how much energy is lost in a collision and, thus, affect at how quickly the medium settles in a static state, e.g., when the silo is filled. Particles with a large restitution coefficient (large damping) separate more after a collision; however, due to the high density of the medium, the steric effects are more important than the influence of a single parameter on the overall behavior of the medium. The tangential overlap $\xi \mathbf{t}_{ij}$ increases while the contact lasts but is truncated to fulfill the Coulomb criterium $F_t \leqslant \mu F_n$, where μ is the friction coefficient.

For the simulation, we fix the values of the Young's modulus Y, Poisson ratio ν, coefficient of restitution e, and friction coefficient μ. These are related to the constants of the force model as follows:

$$k_n = \frac{4}{3} Y^* \sqrt{R^* \xi}, \tag{3}$$

$$\gamma_n = -2\sqrt{\frac{5}{6}} \beta \sqrt{S_n m^*} \geqslant 0, \tag{4}$$

$$k_t = 8 G^* \sqrt{R^* \xi}, \tag{5}$$

$$\gamma_t = -2\sqrt{\frac{5}{6}} \beta \sqrt{S_t m^*} \geqslant 0, \tag{6}$$

$$S_n = 2Y^* \sqrt{R^* \xi}, S_t = 8G^* \sqrt{R^* \xi} \tag{7}$$

$$\beta = \frac{ln(e)}{\sqrt{ln^2(e) + \pi^2}}. \tag{8}$$

The mixed variables are defined as

$$\frac{1}{Y^*} = \frac{1-\nu_1^2}{Y_1} + \frac{1-\nu_2^2}{Y_2}, \tag{9}$$

$$\frac{1}{G^*} = \frac{2(2-\nu_1)(1+\nu_1)}{Y_1} + \frac{2(2-\nu_2)(1+\nu_2)}{Y_2}, \tag{10}$$

$$\frac{1}{R^*} = \frac{1}{R_1} + \frac{1}{R_2}, \frac{1}{m^*} = \frac{1}{m_1} + \frac{1}{m_2}. \tag{11}$$

For this study, the particles are identical with their parameters given by $Y = 5 \times 10^6$ Pa, $\nu = 0.45$, $e = 0.3$, and $R = d/2 = 0.5$ mm. The mass is fixed by setting the density equal to 2500 kg/m^3. The friction coefficient is given three different values $\mu = 0.25, 0.5, 0.75$ in order to carry out a parametric study of the results as a function of the properties of the medium. The friction coefficient is especially influential because it determines the degree of rearrangement between contacting particles. As a consequence, beds of grains with a low value of μ become more compact and denser. Other parameters do not have this influence on the structure of the bed. Thus, the role of the Young's modulus is to prevent grains from interpenetrating each other. It may have a minor influence in the density or packing fraction of the bed, but not in its microstructure. The coefficient of restitution controls the time required to reach a static situation, but it cannot prevent the rearrangements.

The parameter values selected give rise to results that are consistent other computational and experimental studies in the literature (see, e.g., [2,4,5,9,14,23,24,26,32,41,43]). The value chosen for the Young's modulus ensures that the particles are stiff enough to display a realistic granular behavior, while keeping the integration time step δt at manageable values. In the present case $\delta t = 10^{-5}s$, which is 20 times smaller than the average duration of the contact of particles in the vicinity of the outlet size, as estimated from their velocities [44]. However, some simulations have been repeated with an integration time step $\delta t = 5 \times 10^{-6}$ s (and $\mu = 0.5$) to ensure that the results hold.

Finally, we note that the particle-wall interaction is modeled in the same way as particle-particle interactions, but assuming that the second particle has infinite mass and radius (flat wall limit). The material properties of the second particle are the same than those of the bulk particles.

B. Simulation protocol

The protocol used to obtain the results presented in this work is as follows. First, particles are randomly placed inside the silo and given random velocities. Initially, the outlet at the bottom is closed, and particles are allowed to settle under the influence of gravity. The creation and settlement of particles is done in several batches until reaching the desired number of grains. Once the kinetic energy has achieved a negligible value, $E_k \leqslant 10^{-10}$ J, so particles can be considered to be at rest, the outlet is opened and particles flow out. In order to keep the conditions of the discharge constant, after the exiting particles have fallen a distance $4d$ they are reintroduced at the top of the silo.

Although the silo discharge reaches a stationary state rather quickly as monitored, e.g., by the kinetic energy, the simulation is allowed to proceed during several hundred thousand time steps before recording data for analysis. To study the collision frequency, 20 000 consecutive time frames are used. This allows us to record several thousand collision events. To study average quantities such as the packing fraction and the typical velocities, around 1000 time frames separated from each other by 10 000 time steps are used. When using the smaller integration time step, the frequencies are doubled.

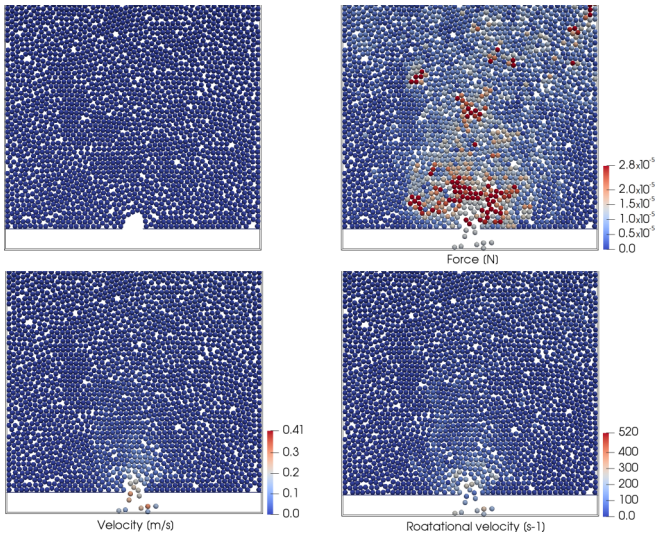

FIG. 2. Snapshots of a simulation with $D = 4d$ and $\mu = 0.5$. Top left: An instance of an arch arresting the flow. Top right: Total force on each particle. Bottom left: Velocity magnitude. Bottom right: Rotational velocities.

For outlet sizes such that stable arches appear ($D \leqslant 5d$), we use the following procedure to identify a clog and remove the arch. Based on trial simulations, when the kinetic energy is below 10^{-10} J (for comparison, this is around four orders of magnitude lower than the steady state kinetic energy), it is safe to say that the flow is arrested. The particles forming the blocking arch are identified by locating those with lowest vertical coordinate whose horizontal position lies within the limits of the outlet. This particles are displaced vertically to a position below the base of the silo in one time step. This has always been observed to be enough to resume the flow.

In Fig. 2, are shown some snapshots of a simulation with $D = 4d$ and $\mu = 0.5$. In the top-left panel there is an instance of an arch. Two particles can be seen "hanging" due to friction. The other three panels show the same time instant, taken a few time steps after the removal of the arch. The top right panel shows the total force on each particle. The forces distribution is very heterogeneous, as is characteristic of granular media [45]. There is a concentration of large forces on particles close to the exit, probably due to particles precipitating to close the space left by the removal of the arch. The bottom left panel shows the velocity magnitude, while the bottom right panel shows the angular velocities. The linear velocities close to the outlet are roughly below 0.2 m/s, decreasing quickly in the bulk. The distribution of rotational velocities is analogous to that of the linear ones.

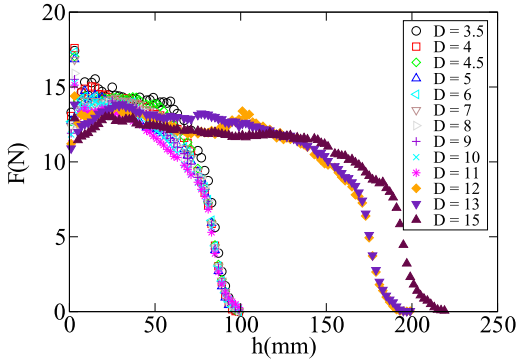

FIG. 3. Janssen effect. Horizontal component of the force exerted on the vertical walls of the silo for all outlet sizes. The data are averages over time during the discharge of the silo.

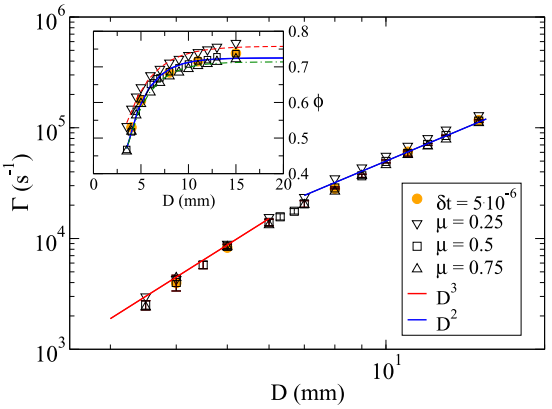

FIG. 4. Collision frequency. Collision frequency as a function of the outlet size. The open symbols represent the main result, while the orange circles are the checking values obtained reducing the integration time step of the simulations, and $\mu = 0.5$. The red and blue lines are fitting lines. Inset: packing fraction in the observation window as a function of the outlet size. The lines are a fit to function Eq. (12).

The Janssen effect in our simulations is shown in Fig. 3. In particular, the plot displays the horizontal force exerted on the vertical walls as a function of the height during the discharge of the silo. The force is zero in the free surface of the silo but rises quickly as the height decreases. After a few tens of particle diameters, the force reaches a quasiplateau in which the force increases very gently. This behavior is entirely similar to that observed in other granular dynamical systems (see, e.g., Refs. [46,47]). Note that all the signals tend to the same value of the force near the bottom, independently of the filling height. The peak observed near the bottom of the silo, that causes a dispersion of the data, is due to the sequential initial filling used. This effect is thoroughly discussed in Ref. [48]. In the present study, particles are allowed to flow until a steady state develops, which erases the memory of the filling protocol.

III. RESULTS AND DISCUSSION

A. Collision rate

Since we are interested in the dynamics of particles close to the outlet, we focus on a square area of size $D \times D$ whose bottom side coincides with the outlet of the silo. More important, inside this window of observation is where most blocking arches form, as has been demonstrated experimentally [49]. To count the number of collisions, the contact matrix (a $N \times N$ matrix whose values are $c_{ij} = c_{ji} = 1$ if particles i and j are in contact and zero otherwise) for all the particles in the simulation is built at each time step. A collision is counted whenever two particles are in contact in time step t_i *and* they were not in contact in the previous time step t_{i-1}. When clogging appears, all the collisions occurred between the removal of one clog and the next are included in the calculation of the collision frequency. Given that the area of the observation window grows with D one would anticipate that the collision frequency Γ scales as D^2. However, as can be seen in Fig. 4, this is only the case for outlet sizes $D \gtrsim 7d$. Below this value, the collision frequency grows more quickly than expected, with an exponent approximately equal to 3. As in the case of the mass flow rate, this can be understood taking into account that the packing fraction ϕ of the particles in the area also grows with D. The inset to Fig. 4 shows the packing fraction computed in the observation window. As has been observed in experimental systems [33,42], the growth behaves as a saturating exponential. The saturation is reached for a value slightly above 0.7. The dependence can be well fitted to a function of the form [34,42]:

$$\phi(D) = a(1 + be^{-D/c}). \tag{12}$$

The fitting parameters are summarized in Table I. The parameter a is the asymptotic value of the packing fraction for large aperture sizes. As discussed above, it decreases monotonically upon increasing the coefficient of friction because higher values of μ prevent the rearrangement of particles in the bed. The parameter c has the dimensions of a distance and its value is between $2d$ and $3d$, with no monotonous dependence on μ. This is consistent with the experimental value of "diffusive constants" derived from fitting the vertical velocity profile measured inside the silo [50–53] to the phenomenological continuous model derived in Ref. [31].

A normalized collision frequency is defined dividing the frequency by the area of the window of observation and the

TABLE I. Parameters from fitting the data in Fig. 4 and Figs. 5(a)–5(c) to Eq. (12).

μ	0.25	0.5	0.75
Parameters from packing fraction Fig. 4			
a [−]	0.758	0.725	0.714
c [mm]	2.74	2.14	2.32
Parameters from collision frequency Fig. 5(a)			
a [s^{-1} mm^{-2}]	759.8	698.7	670.5
c [mm]	1.85	2.65	2.15
Parameters from collision frequency Fig. 5(b)			
a [s^{-1} mm^{-2}]	783.2	726.9	697.3
c [m/s]	0.073	0.075	0.053
Parameters from exit velocity Fig. 5(c)			
γ [−]	1.097	0.993	0.871

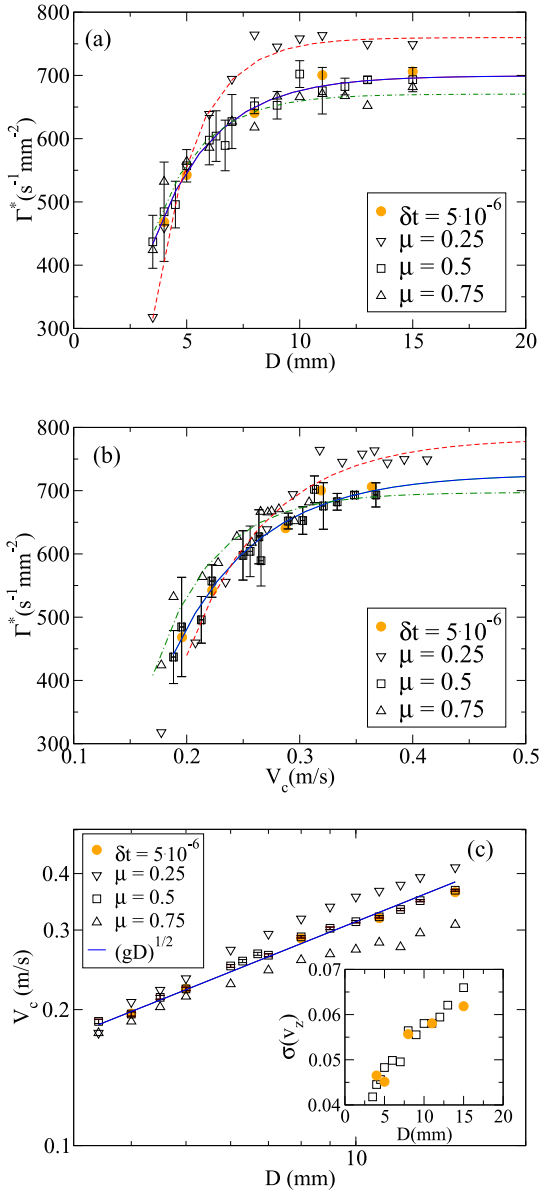

FIG. 5. Normalized collision frequency. Top: Normalized collision frequency as a function of the outlet size. The empty symbols represent the main result, while the orange circles are the checking values obtained reducing the integration time step of the simulations and $\mu = 0.5$. Middle: Normalized collision frequency as a function of the vertical velocity of the particles exiting through the center of the outlet. The continuous lines are fits to function Eq. (12). Bottom: Vertical velocity of the particles exiting through the center of the outlet as a function of the outlet size. Inset: Variance of the velocity of particles inside the observation window.

packing fraction $\Gamma^* = \frac{\Gamma}{D^2\phi}$. In this way, we take into account the increasing size of the window of observation and the varying packing fraction. Note that $D^2\phi$ is approximately the number of particles inside that window. This normalized collision frequency is plotted in Fig. 5(a). The results obtained with the three values of μ are reported but only the error bars of the case $\mu = 0.5$ are shown, the others being similar. The collision frequency is found to grow for small values of the outlet size. The rate of growth starts to decrease around $D = 7d$ and it finally reaches a saturating value near $D = 10d$. The data can be fitted to a function of the same form than Eq. (12). In this case, the value of the characteristic length is $c \approx 2d$ again (see Table I), which is consistent with the value derived from the behavior of the packing fraction. Note that the lower the packing fraction of the bed corresponds to the lower the value of the normalized collision frequency, since there are fewer particles to provoke collisions. This trend is observed with respect to the friction coefficient as well: For a high value of μ the curve is lower because the bed is less dense, while for the lower value of μ the curve moves upward. It should be noted that the dependence of the collision frequency on the outlet size is the same if one uses $\Gamma^* = \Gamma/D^2$ instead of $\Gamma^* = \Gamma/(\phi D^2)$; only the values change. So, this dependence is not an artifact of dividing by ϕ. The formal similarity of the curves in Figs. 4 and 5(a) strongly suggests a relationship of the former result to the behavior of the packing fraction, although other effects might play a role.

In Fig. 5(b), the normalized frequency is plotted against the vertical velocity of the particles flowing out through the center of the outlet $V_c = V_z(W/2, 0, 0)$. This velocity is chosen as a characteristic velocity because the vertical velocity of the particles changes inside the $D \times D$ window as they fall. The advantage of V_c is that it has a predictable value [32,42] very approximately given by $\sqrt{\gamma gD}$, where g is the acceleration of gravity and γ is a parameter whose value is close to 1. As can be seen in Fig. 5(c), the fit is very close for $\mu = 0.5$, while the exit velocity is slightly higher and slightly lower for lower and higher friction, respectively. Additionally, the range of values spanned by V_c is wider than that of the average vertical velocity in the box or the average speed, which makes the result easier to visualize. Although the saturation is not as clear as in the case of Γ^* versus D, the data points are fitted with the same saturating exponential Eq. (12). The characteristic velocity given by the fitting parameter c is $V_c^* \approx 0.075$ m/s. This value corresponds with those experimentally found in the bulk of the silo [8,43,52–54]. Additionally, the values of γ further stress consistency with experiments [32,42].

This result is very surprising. Intuitively, one would expect to see an increase in the collision rate of the particles upon increasing their velocities [55,56]. Although the silo is an open system, we have seen that the space available for particles shrinks upon increasing D. However, the collision rate increases only up to moderate values of the outlet size $D \lesssim 7d$. Onward, the collision rate flattens in spite of the velocity's continuous increase. Interestingly, the so-called granular temperature, given by the variance of the velocity [57], also increases monotonically [see inset to Fig. 5(c)] in a linear fashion. This means that the agitation of the particles is not enhancing the probability of collisions either. It appears that the collision rate only increases while the area around the outlet is being filled with particles, as measured by the packing fraction in order to compare the increasing areas.

The new result shown in Figs. 5(a) and 5(b) has implications for the probability of arch formation and clogging. The number of particles in a clogging arch grows linearly with D [49].The chance encounter of a growing number of particles should hence decrease with D. This intuition is made a strong argument in Ref. [38], where it is shown that the number of

configurations of grains near the exit that cause a clog falls exponentially upon increasing the outlet size. Hence, the flow needs to sample an exponentially large number of grains' configurations before finding one able to block the exit. Our result implies that this sampling is hindered by the saturation in the collision rate that results from filling with particles the area near the outlet. This strengthens the conclusion than when increasing the outlet size clogs are possible but extremely unlikely.

Furthermore, the continuity of the curve Γ^* versus D suggests that there is no critical outlet size. Instead, the transition from the clogging to the continuous flow regime is smooth.

B. Distribution of velocities

In order to explore further the dynamics of the colliding particles near the exit, we compute the probability distribution functions (PDF) of the horizontal and vertical instantaneous velocities. For clarity of the plots, we report values for $\mu = 0.5$. These are shown in Figs. 6(a) and 6(b), respectively with the velocities normalized by their standard deviation. The distribution of horizontal velocities follows excellently a Gaussian shape for all values of D. Note that there is no fit to the data due to the normalization applied. This result is natural since there are no forces or other influences in the horizontal direction. To build the PDF of the vertical velocities, the average is computed inside the window of observation and subtracted from the instantaneous velocity of each particle. This PDF deviates from a Gaussian in two ways. First, the tails of the distribution show an overpopulation of downward (negative) velocities and a depletion of upward (positive) velocities. This result is natural given that most particles are effectively falling and that the average is not constant inside the window (it varies with the vertical coordinate). Second, close to the center of the distribution the opposite trend appears: The positive velocities are enhanced while the negative ones are depleted. This is due to the collisions between the particles. Effectively, when particles enter the observation window, their accelerations and velocities are minimal [32], and hence collisions are more likely to produce large deviations in the velocity vectors. When particles have fallen some distance inside the window and built up greater acceleration, they are more difficult to deviate.

Previous works [53,58,59] have reported non-Gaussian velocities for individual particles in a silo. All those works carried out their measurements in the bulk of the silo, instead of in the vicinity of the exit. As has been discussed in the introduction, the dynamics in that region is dominated by lasting contacts due to the larger density of the medium. This enhances the correlations between particles [53] which give rise to deviations from the Gaussian in the PDFs of velocities and displacements. Indeed, in Ref. [53] it can be seen that as one approaches the bottom of the silo the non-Gaussian features of the distribution of particles' velocities wear off. Comparing Fig. 6 with the experimental results in, e.g., Refs. [51–53] one can see that, again, the presented simulations are consistent with the experimentally measured behavior of particles in a silo.

In Figs. 6(a) and 6(b), the velocities refer to individual particles. We also compute the average over particles in the $D \times$

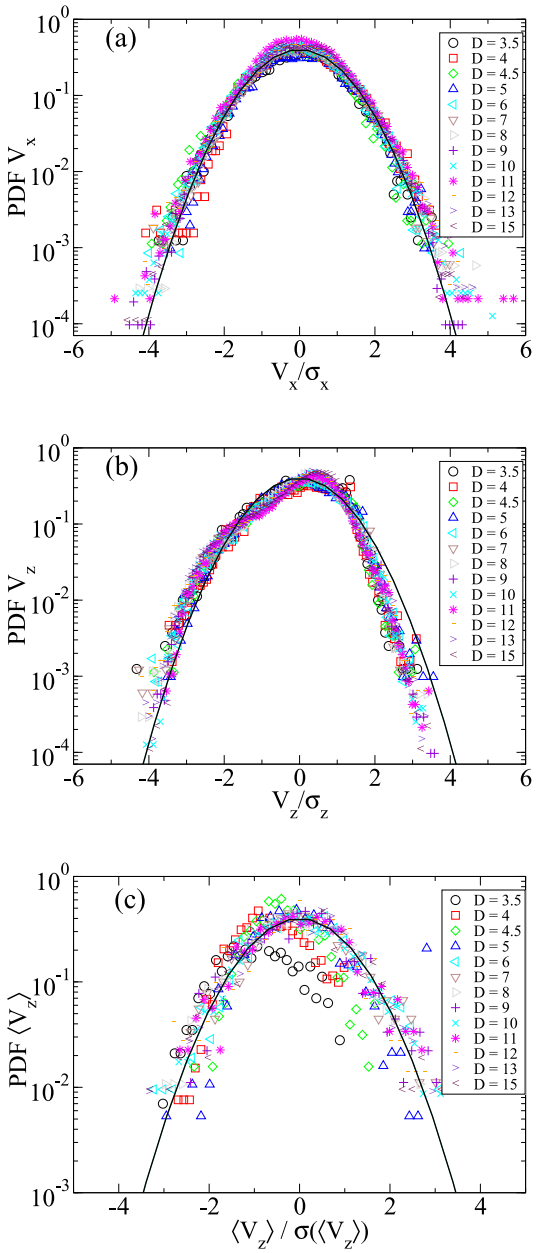

FIG. 6. Velocity histograms. Top: Probability distribution function of the horizontal velocities of individual particles. Middle: Probability distribution function of the vertical velocities of individual particles, subtracting the average in the window. Bottom: Probability distribution function of the fluctuations of the average vertical velocity computed in the window of observation. The distributions are normalized and the velocities rescaled by the standard deviation. The black line is a Gaussian function with average equal to zero and standard deviation equal to the unity. There is no fit in the plots.

D window during several seconds. This average fluctuates over time but has a well-defined stationary value. Subtracting the stationary value from the instantaneous average in each time step, we obtain the fluctuations of the average velocity. This is displayed in Fig. 6(c) for the vertical component. The distribution is Gaussian in all cases, only showing deviations for the smallest values of outlet $D \leqslant 4.5d$. Note that for these

values the clogs are so frequent that the time series to be used to produce the histograms are very short. Besides, the data present a rather wide oscillation inside each time series. Both effects preclude obtaining a well-defined average. However, the result shown is consistent with the measurements presented in Ref. [53], where the fluctuations of the average velocity magnitude are found to be Gaussian. The deviations in the result for small orifices is due to lack of statistics. Effectively, the size of the window is very small in these cases, housing a very small number of particles compared to larger apertures.

The conclusion presented at the end of Sec. III A regarding the absence of evidence of a critical outlet size is further reinforced by the results just discussed. The PDFs shown in Fig. 6, once normalized, are all the same for small and large apertures. In the horizontal direction, they are perfectly Gaussian, as expected. The deviation from Gaussianity in the vertical component of individual particles can be explained by the collisional dynamics in the vicinity of the outlet. Finally, the fluctuations of the average are Gaussian, in agreement with experiments, for all outlets. This indicates that the dynamics of particles in the region near the exit, where blocking arches form, is unaffected by the increasing area of the outlet.

C. Distribution of time lags

We now study the time lag ΔT_L between successive collisions. The PDFs for all cases with $\mu = 0.5$ are shown in Fig. 7(a). The distributions roughly follow a power law distribution falling with an exponent equal to 2. However, there are differences. First, short time lags are more likely in the cases of large apertures. Second, the trend reverses for larger ΔT_L, which are less likely for large D. This observation has an intuitive explanation based on the results presented for the packing fraction (see Fig. 4). In the case of a small window of observation, the packing fraction is low and particles can travel longer distances between collisions. As D increases, so does the packing fraction and, consequently, the time between successive collisions shortens. Additionally, the velocity of the particles is lower for lower values of D [see Fig. 5(c)].

In Fig. 7(b), we show the time lag distributions for a few values of D for which simulations were carried out with a reduced integration time step. The values displayed change slightly, but the general conclusions remain unchanged. Reducing the integration time increases the probability to observe large time lags. Instead, the frequency of short lag times is corrected by a very small amount.

The behavior of the normalized average time lag $T_L^* = T_L D^2 \phi$ as a function of the aperture size and the friction coefficient is shown in Fig. 7(c). As deduced from the histograms, the time lag is larger for small values of D and decreases upon increasing D. More interesting, there is a saturation for $D \gtrsim 10d$ above which the curve flattens. This behavior is concomitant with the saturation of the packing fraction and the collision frequency discussed earlier. The influence of the friction coefficient on the curves is reversed with respect to the collision frequency curves.

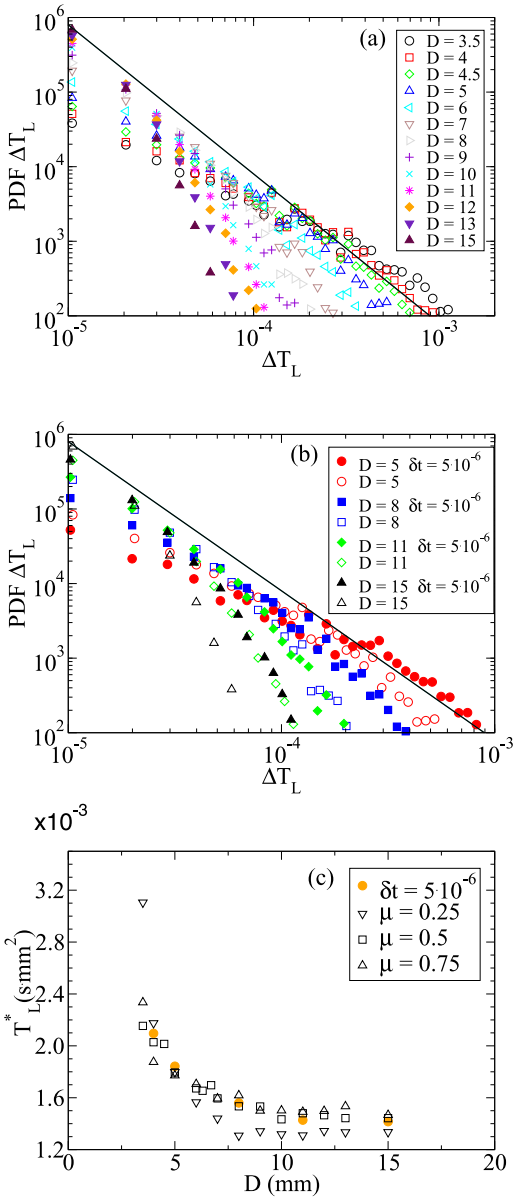

FIG. 7. Time lag statistics. Top: Probability distribution function of the time lags between successive collisions. Middle: Same distributions obtained from simulations using a shorter integration time step and compared with the originals displayed in the left panel. The black lines are guides to the eye with a slope equal to −2. Bottom: Average normalized time lag $\Delta T_L^* = \Delta T_L \times D^2 \times \phi$ as a function of the outlet size.

IV. CONCLUSION

This work analyses the behavior of particles in a silo in the region close to the outlet. The dynamics in this region is characterized by a collisional regime, in which contacts are short-lived. This is in contrast with the bulk of the silo where contacts are permanent or long-lived. Interestingly, it is in this region where the arches that block the exit and arrest the flow (for outlet sizes $D \lesssim 5d$) are formed [49]. The study covers a range of outlet sizes D from small ones, where arches appear frequently and is necessary to remove them, to big apertures for which flow is continuous. It has been shown that the collision frequency of the particles increases with D until it reaches a saturation value and flattens from $D \approx 10d$ onward. This is coincident with the saturation of the packing fraction

which, as had been previously observed, behaves similarly. The same behaviour is obtained when the collision frequency is studied as a function of the velocity of the particles. This is puzzling given that the velocity increases continuously and one would expect to see more frequent collisions upon greater velocities [55,56].

The main result holds when the friction coefficient of the particles changes. This material coefficient results in a denser packing when it is small because it allows particles to rearrange. When the friction takes high values particles get interlocked more easily and the density of the bulk medium decreases. The consequence for the collision frequency is that it increases for the lower value of μ because the chances of encounter between particles increase. Instead, when the friction coefficient is raised the collision frequency decreases because particles have more space available to move.

The saturation of the collision frequency has consequences for the existence of a critical outlet size from which arches never appear. In the frame of the statistical argument put forward in Ref. [38], the flattening of the collision frequency implies a reduced number of chance encounters between particles and, consequently, a reduced ability of the flow to sample configurations compatible with a clog.

Furthermore, the analysis of the distribution functions of the velocities shows no transition in respect to the outlet size. Tellingly, the histograms of the individual velocities are Gaussian for both horizontal and vertical components and for all values of D. The small deviations present in the histogram of the vertical velocity (the average subtracted) are easily accountable by the dynamics of collisions. The PDF of the fluctuations around the stationary value of the average (over particles) vertical velocity is a Gaussian as well, consistent with experiments [49].

To complete the study of the collisional regime, the time lag has been analyzed. It is found that the time lag distribution follows roughly a power law decay with exponent 2. This general trend is nuanced by a depletion of short time lags for small apertures and, conversely, a depletion of long time lags for large outlet sizes. This is consistent with the behavior of the packing fraction and the collision frequency. Interestingly, the average time lag does not just decrease, upon increasing D, it reaches a plateau in a similar (but inverted) fashion as the collision frequency.

In conclusion, the collisional dynamics of particles does not show evidence of critical behavior respect to the outlet size. Furthermore, it is worth noting that the change of behavior (the transition to a plateau) of the collision frequency and the time lag occur at a value of $D \gtrsim 7d$ larger than that for which arches start to appear $D \lesssim 5d$. It is difficult to harmonize this observation with the existence of a critical D which separates the continuous flow regime from the clogging regime. It is consistent, instead, with a gradual decrease in the probability to observe clogs as the size of the outlet increases.

The next logical extension of the present work would be to run simulations in $3D$ to study the influence of dimensionality. Many of the characteristics of the flow of granular matter inside a silo are analogous in $2D$ and $3D$, including the existence of clogging and continuous regimes, the variation of the flow with the outlet size, the variation of the packing fraction, the saturation of pressure, the velocity profiles of the particles, and the PDF of the velocities. However, dimensionality could have an influence on the existence of some behaviors. In this regard, it has been suggested [36] that this variable could have an influence on the existence of a putative critical outlet size.

The results in the literature show that both in $2D$ and $3D$ the outlet size defines the relevant length scale and that it can be conveniently made dimensionless by the typical size of the flowing particles. Having a dimensionless number allows to carry the results to systems of different size. Effectively, the engineering literature shows that interesting magnitudes such as the flow, pressure, and velocities behave in the same way as in laboratory setups or simulations. Hence, the results reported in this work should be observable in industrial-scale silos because they depend on the D/d ratio of outlet to particle size. Of course, for practical reasons, industrial-scale silos usually operate in the regime $D \gg d$, precisely to avoid clogging-related problems.

ACKNOWLEDGMENTS

This work has been supported by European Union's Horizon 2020 Research and Innovation Programme under the Grant Agreement No. 820771 (BAMBOO Project). I thank my colleague Ana González-Espinosa for critical reading of an early version of the manuscript.

[1] K. To, P.-Y. Lai, and H. K. Pak, Jamming of Granular Flow in a Two-Dimensional Hopper, Phys. Rev. Lett. **86**, 71 (2001).

[2] X. Li, J. Wan, S. Zhang, P. Lin, Y. Zhang, G. Yang, M. Wang, W. Duan, J. Sun, and L. Yang, Preliminary research on flow rate and free surface of the accelerator driven subcritical system gravity-driven dense granular-flow target, PLoS ONE **12**, e0187435 (2017).

[3] F. Alonso-Marroquín and P. Mora, Beverloo law for hopper flow derived from self-similar profiles, Gran. Matter **23**, 7 (2021).

[4] Y. Zhou, P. Ruyer, and P. Aussillous, Discharge flow of a bidisperse granular media from a silo: discrete particle simulations, Phys. Rev. E **92**, 062204 (2015).

[5] X. Yang, N. Gui, J. Tu, and S. Jiang, Numerical analysis of granular flows in a silo bed on flow regime characterization, PLoS ONE **10**, e0119155 (2015).

[6] F. Alonso-Marroquín, A. Ramírez-Gomez, C. González-Montellano, N. Balaam, D. A. H. Hanaor, E. A. Flores-Johnson, Y. Gan, S. Chen, and L. Shen, Experimental and numerical determination of mechanical properties of polygonal wood particles and their flow analysis in silos, Gran. Matter **15**, 811 (2013).

[7] A. Ashour, T. Trittel, T. Börzsönyi, and R. Stannarius, Silo outflow of soft frictionless spheres, Phys. Rev. Fluids **2**, 123302 (2017).

[8] L. A. Fullard, C. E. Davies, A. C. Neather, E. C. P. Breard, A. J. R. Godfrey, and G. Lube, Testing steady and transient velocity scalings in a silo, Adv. Powder Tech. **29**, 310 (2018).

[9] J. Wan, F. Wang, G. Yang, S. Zhang, M. Wanga, P. Lin, and L. Yang, The influence of orifice shape on the flow rate: A DEM and experimental research in 3D hopper granular flows, Powder Technol. **335**, 147 (2018).

[10] R. C. Hidalgo, A. Goni-Arana, A. Hernández-Puerta, and I. Pagonabarraga, Flow of colloidal suspensions through small orifices, Phys. Rev. E **97**, 012611 (2018).

[11] S. D. Liu, Z. Y. Zhou, R. P. Zou, D. Pinson, and A. B. Yu, Flow characteristics and discharge rate of ellipsoidal particles in a flat bottom hopper, Powder Technol. **253**, 70 (2014).

[12] C. A. Calderón, M. C. Villagrán-Olivares, R. O. Uñac, and A. M. Vidales, Correlations between flow rate parameters and the shape of the grains in a silo discharge, Powder Technol. **320**, 43 (2017).

[13] P. Peralta, M. Aguirre, J.-C. Géminard, and L. A. Pugnaloni, Apparent mass during silo discharge: Nonlinear effects related to filling protocols, Powder Technol. **311**, 265 (2017).

[14] J. R. Darias, M. A. Madrid, and L. A. Pugnaloni, Differential equation for the flow rate of discharging silos based on energy balance, Phys. Rev. E **101**, 052905 (2020).

[15] R. Caitano, B. V. Guerrero, R. E. R. González, I. Zuriguel, and A. Garcimartín, Characterization of the Clogging Transition in Vibrated Granular Media, Phys. Rev. Lett. **127**, 148002 (2021).

[16] S. F. Edwards, *Granular Matter: An Interdisciplinary Approach* (Springer, New York, 1994).

[17] L. P. Kadanoff, Built upon sand: Theoretical ideas inspired by granular flows, Rev. Mod. Phys. **71**, 435 (1999).

[18] F. Vahidi-Nia, H. Bayesteh, and M. Khodaparast, Effect of initial packing density, stress level and particle size ratio on the behavior of binary granular material: a micromechanical approach, Gran. Matter **22**, 68 (2020).

[19] S. Lévay, D. Fischer, R. Stannarius, B. Szabó, T. Börzsönyi, and J. Török, Frustrated packing in a granular system under geometrical confinement, Soft Matter **14**, 396 (2018).

[20] J. A. Dijksman, L. Kovalcinova, J. Ren, R. P. Behringer, M. Kramar, K. Mischaikow, and L. Kondic, Characterizing granular networks using topological metrics, Phys. Rev. E **97**, 042903 (2018).

[21] M. Baldovin, A. Puglisi, and A. Vulpiani, Langevin equations from experimental data: The case of rotational diffusion in granular media, PLoS ONE **14**, e0212135 (2015).

[22] Y. Grasselli and H. J. Herrmann, Shapes of heaps and in silos, Eur. J. Phys. B **10**, 673 (1999).

[23] C. González-Montellano, A. Ramírez, J. M. Fuentes, and F. Ayuga, Numerical effects derived from en masse filling of agricultural silos in DEM simulations, Comput. Electron. Agr **81**, 113 (2012).

[24] T. Li, H. Zhang, M. Liu, Z. Huang, H. Bo, and Y. Dong, DEM study of granular discharge rate through a vertical pipe with a bend outlet in small absorber sphere system, Nucl. Eng. Des **314**, 1 (2017).

[25] K. Saleh, S. Golshan, and R. Zarghami, A review on gravity flow of free-flowing granular solids in silos—Basics and practical aspects, Chem. Eng. Sci. **192**, 1011 (2018).

[26] T. Tian, J. Su, J. Zhan, S. Geng, G. Xu, and X. Liu, Discrete and continuum modeling of granular flow in silo discharge, Particuology **36**, 127 (2018).

[27] H. A. Janssen, Versuche über Getreidedruck in Silozellen, Zeitschr. d. Vereines deutscher Ingenieure **39**, 1045 (1895).

[28] W. A. Beverloo, H. A. Leniger, and J. J. V. de Velde, The flow of granular solids through orifices, Chem. Eng. Sci. **15**, 260 (1961).

[29] R. O. Uñac, A. M. Vidales, O. A. Benegas, and I. Ippolito, Experimental study of discharge rate fluctuations in a silo with different hopper geometries, Powder Technol **225**, 214 (2012).

[30] R. M. Nedderman, *Statics and Kinematics of Granular Materials* (Cambridge University Press, Cambridge, UK, 1992).

[31] R. M. Nedderman and U. Tüzün, A kinematic model for the flow of granular materials, Powder Technol. **22**, 243 (1979).

[32] S. M. Rubio-Largo, A. Janda, D. Maza, I. Zuriguel, and R. C. Hidalgo, Disentangling the Free-Fall Arch Paradox in Silo Discharge, Phys. Rev. Lett. **114**, 238002 (2015).

[33] I. Zuriguel, A. Janda, A. Garcimartín, C. Lozano, R. Arévalo, and D. Maza, Silo Clogging Reduction by the Presence of an Obstacle, Phys. Rev. Lett. **107**, 278001 (2011).

[34] C. Mankoc, A. Janda, R. Arévalo, J. Pastor, I. Zuriguel, A. Garcimartín, and D. Maza, The flow rate of granular materials through an orifice, Gran. Matter **9**, 407 (2007).

[35] I. Zuriguel, A. Garcimartín, D. Maza, L. A. Pugnaloni, and J. M. Pastor, Jamming during the discharge of granular matter from a silo, Phys. Rev. E **71**, 051303 (2005).

[36] A. Janda, I. Zuriguel, A. Garcimartín, L. A. Pugnaloni, and D. Maza, Jamming and critical outlet size in the discharge of a two-dimensional silo, Europhys. Lett. **84**, 44002 (2008).

[37] K. To, Jamming transition in two-dimensional hoppers and silos, Phys. Rev. E **71**, 060301(R) (2005).

[38] C. C. Thomas and D. J. Durian, Fraction of Clogging Configurations Sampled by Granular Hopper Flow, Phys. Rev. Lett. **114**, 178001 (2015).

[39] C. Kloss, C. Goniva, A. Hager, S. Amberger, and S. Pirker, Models algorithms and validation for open source DEM and CFD-DEM, Prog. Comput. Fluid **12**, 140 (2012).

[40] S. Plimpton, Fast parallel algorithms for short-range molecular dynamics, J. Comp. Phys **117**, 1 (1995).

[41] D. Hirshfeld and D. C. Rapaport, Granular flow from a silo: Discrete-particle simulations in three dimensions, Eur. Phys. J. E **4**, 193 (2001).

[42] A. Janda, I. Zuriguel, and D. Maza, Flow Rate of Particles Through Apertures Obtained from Self-Similar Density and Velocity Profiles, Phys. Rev. Lett. **108**, 248001 (2012).

[43] C. González-Montellano, F. Ayuga, and J. Y. Ooi, Discrete element modelling of grain flow in a planar silo: Influence of simulation parameters, Gran. Matter **13**, 149 (2011).

[44] J. Schäfer, S. Dippel, and D. E. Wolf, Force schemes in simulations of granular materials, J. Phys. I (France) **6**, 5 (1996).

[45] T. S. Majmudar and R. P. Behringer, Contact force measurements and stress-induced anisotropy in granular materials, Nature (London) **423**, 1079 (2005).

[46] Y. Bertho, F. Giorgiutti-Dauphiné, and J.-P. Hulin, Dynamical Janssen Effect on Granular Packing with Moving Walls, Phys. Rev. Lett. **90**, 144301 (2003).

[47] C. R. K. Windows-Yule, S. Mühlbauer, L. A. Torres Cisneros, P. Nair, V. Marzulli, and T. Pöschel, Janssen effect in dynamic particulate systems, Phys. Rev. E **100**, 022902 (2019).

[48] S. Mahajan, M. Tennenbaum, S. N. Pathak, D. Baxter, X. Fan, P. Padilla, C. Anderson, A. Fernandez-Nieves, and M. Pica

Ciamarra, Reverse Janssen Effect in Narrow Granular Columns, Phys. Rev. Lett. **124**, 128002 (2020).

[49] A. Garcimartín, I. Zuriguel, L. A. Pugnaloni, and A. Janda, Shape of jamming arches in two-dimensional deposits of granular materials, Phys. Rev. E **82**, 031306 (2010).

[50] J. Choi, A. Kudrolli, R. R. Rosales, and M. Z. Bazant, Diffusion and Mixing in Gravity-Driven Dense Granular Flows, Phys. Rev. Lett. **92**, 174301 (2004).

[51] J. Choi, A. Kudrolli, and M. Z. Bazant, Velocity profile of granular flows inside silos and hoppers, J. Phys-Cond. Matter **17**, S2533 (2005).

[52] I. Zuriguel, D. Maza, A. Janda, R. C. Hidalgo, and A. Garcimartín, Velocity fluctuations inside two and three dimensional silos, Gran. Matter **21**, 47 (2019).

[53] A. Garcimartín, I. Zuriguel, A. Janda, and D. Maza, Fluctuations of grains inside a discharging two-dimensional silo, Phys. Rev. E **84**, 031309 (2011).

[54] M. Benyamine, M. Djermane, B. Dalloz-Dubrujeaud, and P. Aussillous, Discharge flow of a bidisperse granular media from a silo, Phys. Rev. E **90**, 032201 (2014).

[55] E. Falcon, S. Aumaître, P. Évesque, F. Palencia, C. Lecoutre-Chabot, S. Fauve, D. Beysens, and Y. Garrabos, Collision statistics in a dilute granular gas fluidized by vibrations in low gravity, EPL **74**, 830 (2006).

[56] S. Aumaître and S. Fauve, Collision frequencies and energy flux in a dilute granular gas, Phys. Rev. E **73**, 010302(R) (2006).

[57] C. K. K. Lun, S. B. Savage, D. J. Jeffrey, and N. Chepurniy, Kinetic theories for granular flow: Inelastic particles in Couette flow and slightly inelastic particles in a general flow field, J. Fluid. Mech **140**, 223 (1984).

[58] S. Moka and P. R. Nott, Statistics of Particle Velocities in Dense Granular Flows, Phys. Rev. Lett. **95**, 068003 (2005).

[59] R. Arévalo, A. Garcimartín, and D. Maza, Anomalous diffusion in silo drainage, Eur. Phys. J. E **23**, 191 (2007).